International Journal of Hydrogen Energy 154 (2025) 150120

Contents lists available at ScienceDirect

International Journal of Hydrogen Energy

journal homepage: www.elsevier.com/locate/he

Understanding deactivation and reactivation of oxidation catalysts in hydrogen combustion engines

Alexander Lampkowski [a,*], Stefan Sterlepper [a], Maike Schäfer [a], Sebastian Roiser [b], Christian Tomanik [c], Helmut Eichlseder [b], Stefan Pischinger [a]

[a] Thermodynamics of Mobile Energy Conversion Systems, RWTH Aachen University, Germany
[b] Institute of Thermodynamics and Sustainable Propulsion Systems, Technical University of Graz, Austria
[c] Umicore AG & Co. KG, Germany

ARTICLE INFO

Keywords:
Oxidation catalyst
Deactivation
Exhaust gas aftertreatment
Hydrogen
Internal combustion engine
Cold start

ABSTRACT

This research investigates the deactivation phenomena of oxidation catalysts in exhaust gas aftertreatment systems of hydrogen internal combustion engines (H_2-ICEs). The study observes an unexpected catalyst deactivation during extended cold start operation, which is partially reversible through lambda variation and increased exhaust temperatures. Light-off tests on a synthetic gas bench (SGB) reproduce these deactivation effects during the absence of carbon-based and nitrogen oxide emissions, showing that preconditioning with nitrogen oxide (NO) can aid partial reactivation. Additionally, conditioning at higher temperatures effectively prevents significant deactivation. The findings suggest that state-of-the-art oxidation catalysts from diesel engines are applicable for H_2-ICEs if suitable engine operating modes are employed to mitigate catalyst deactivation.

1. Introduction

Hydrogen internal combustion engines (H_2-ICEs) powered by green hydrogen enable climate-neutral drives as a solution to limit the climate change [1,2]. Compared to battery electric systems, H_2-ICEs have the advantage of fast recharging times. Different from PEM fuel cell systems, they are very resistant against fuel impurities, air contamination or varying ambient conditions. Besides, the waste heat is on a higher temperature level and can either be utilized or with high shares be dissipated through the exhaust gas without active cooling. As a result, H_2-ICEs are a competitive propulsion system for long-haul trucks, off-road machinery and other heavy-duty applications [3]. In these applications, high life time performance and high durability are key aspects that have to be guaranteed, not only for the engine itself, but also for the exhaust aftertreatment system [4].

The most significant raw emission species for hydrogen ICEs are nitrogen oxides (NO_x) [5]. Luo et al. [6] observed NO_x concentrations reaching up to $\psi_{NO_x} = 7,000$ ppm at an air-fuel equivalence ratio of $\lambda = 0.88$. State-of-the-art exhaust aftertreatment (EAT) systems for lean-operated ICEs typically consist of an oxidation catalyst (OC) and a selective catalytic reduction (SCR) system using ammonia (NH_3) as the reducing agent. As described by Srisailam et al. [7], such systems – originally developed for diesel engines – can serve as the basis for potential adaptations to H_2-fueled ICEs. Furthermore, Rezaei et al. [8] evaluated various EAT configurations, with two out of the three systems relying on a combination of OC and SCR components. Additionally, H_2-SCR systems are being investigated, but still object of research [9–11]. The NH_3-SCR catalyst performance is often in focus (e.g. investigated in [12] for H_2-ICE exhaust), but also the OC is essential for the EAT as it serves several key functions. In a first function, OCs oxidize potential CO and hydrocarbon (HC) emissions. With hydrogen as a fuel, the single source of carbon-based raw emissions is oil consumption, but still they require action to achieve zero-impact tailpipe emissions [13]. Another key aspect is the partial oxidation of engine-out NO into NO_2, ideally towards a ratio of $NO_2/NO_x = 0.5$. This enables the so called "fast SCR" reaction and thus effective use of the downstream SCR catalyst [14–17].

Another important aspect is the necessity of the OC for hydrogen (H_2) oxidation to avoid false lambda sensor signals due to hydrogen cross-sensitivity [18]. These deviations may also negatively affect the engine calibration [19]. Finally, the OC can also be used for accelerated heat-up after cold-start, where it oxidizes H_2 and thus provides exothermic energy [20].

1.1. Fundamental catalyst deactivation mechanism

The application of catalysts within the exhaust aftertreatment system may result in their deactivation due to various factors. Although

* Corresponding author.
E-mail address: lampkowski@tme.rwth-aachen.de (A. Lampkowski).

https://doi.org/10.1016/j.ijhydene.2025.150120
Received 19 November 2024; Received in revised form 29 May 2025; Accepted 20 June 2025
Available online 5 July 2025

Table 1
Catalyst deactivation mechanisms published by Bartholomew [21].

Type	Mechanism
Chemical	Poisoning Vapor formation Vapor-solid reaction Solid–solid reaction
Mechanical	Fouling Attrition/crushing
Thermal	Thermal degradation

deactivation is unavoidable in most cases, various measures can be taken to slow down the process or avoid some effects [21–23]. The deactivation of catalysts for heterogeneous catalysis leads to a reduction in catalytic activity and, in certain cases, to a reduction in selectivity [21,22]. The associated loss in activity and selectivity could result in an increase in tailpipe and secondary emissions. These mechanisms, adapted from Bartholomew [21], can be classified into three main categories: chemical, mechanical, or thermal deactivation. This classification is presented in Table 1.

The chemical deactivation comprises poisoning of the catalyst, vapor formation and vapor-solid and solid–solid reactions. Poisoning of a catalyst is defined as chemisorption of various species on the active sites [21,22]. Thus, the chemisorption of these species can lead to a loss in activity by blocking active sites, affect the adsorptivity of another species, or alter the electronic or geometric structure of the active sites [21,22]. Moreover, the active sites can be converted into volatile compounds, which then can ultimately be carried out of the catalyst by the exhaust gas flow [24,25]. Additionally, vapor-solid or solid–solid reactions can contribute to the reduction in activity due to the formation of inactive phases from active sites [21,24]. In comparison to catalyst poisoning caused by chemisorption of various species, fouling as a mechanical deactivation mechanism defines blockage by the physical deposition of species from the liquid phase [21,24,26]. These deposits cover and block the active sites as well as the pores of the surface. Mechanical load on the catalyst or high-velocity fluid flow are potential causes of damage to the catalyst, resulting in the crushing or erosion of the monolith and the subsequent loss of the catalytic active material [21,22,25]. Moreover, thermal deactivation occurs at high temperatures primarily via two different sintering processes, resulting in alteration of the active sites. The sintering of active sites, also referred to as crystallite growth, can lead to a reduction in the active surface area [27]. Another sintering process is defined by the deformation of the washcoat or substrate. Thus, resulting in a reduction of the support surface area or an enclosure of active sites due to the collapse of pores [21,22].

1.2. Deactivation phenomenon during cold start tests of hydrogen engines

An oxidation catalyst with a volume of $V_{cat} = 0.8$ l and a platinum loading of $\rho_{load} = 25$ g/ft^3 was tested at the engine test bench facilities of the Institute of Thermodynamics and Sustainable Propulsion Systems (ITnA) of the Graz University of Technology. The OC was fit to a state-of-the-art in-line four-cylinder spark-ignited direct-injection turbocharged hydrogen engine with a displacement of $V_h = 2$ l. Detailed information on the measurement setup can be found in previous publications [12].

Fig. 1 illustrates the hydrogen conversion efficiency η_{H_2} which was subjected to continuous monitoring at an engine speed of $n_{eng} = 1000\,min^{-1}$ and a brake mean effective pressure of $BMEP_{eng} = 10$ bar. The H_2 conversion efficiency η_{H_2} is calculated according to Eq. (1). For the calculation, the H_2 concentration upstream of the sample is defined as $\psi_{H_{2,US}}$, while the concentration downstream of the sample is defined as $\psi_{H_{2,DS}}$.

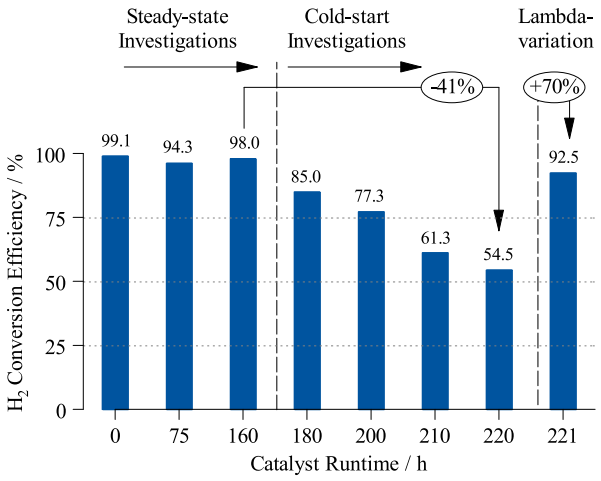

Fig. 1. Hydrogen reduction rates of the oxidation catalyst during its runtime with frequent cold starts and following regeneration due to lambda variation; engine test bench operated at $n_{eng} = 1000\,min^{-1}$ and $BMEP_{eng} = 10$ bar.

$$\eta_{H_2} = \frac{\psi_{H_2,US} - \psi_{H_2,DS}}{\psi_{H_2,US}} \quad (1)$$

During steady-state investigations, which took place in the first $t = 160$ h of the catalyst runtime, the H_2 conversion efficiency η_{H_2} remained relatively stable with values consistently above $\eta_{H_2} > 94\%$. The catalyst runtime defines the duration of engine operation. Subsequently, the catalyst was employed to undertake a series of cold-started driving cycles. A detailed explanation of the pre-conditioning procedure for the engine and the catalyst can be found in [28]. The tests, which included the Worldwide Harmonized Light Vehicles Test Cycle (WLTC) and synthetic Real Driving Emissions (RDE) cycles, were started at $T = 23$ °C ambient temperature without external heating or cooling of the engine or the catalyst. After the driving cycle was completed, pre-conditioning was started again for the follow-up run. In a relatively brief additional runtime of $t = 60$ h, the H_2 conversion efficiency η_{H_2} exhibited a significant decline, dropping from $\eta_{H_2} = 98\%$ to 54.5%. Consequently, the decline led to a substantial increase in H_2 emissions. This observation is not in line with previous experience at lean diesel EAT systems and suggests the emergence of an unidentified deactivation phenomenon.

Due to the unexpected level of the catalyst efficiency reduction, the question arises: What are significant differences of the H_2-ICE setup to conventional diesel ICE exhaust? First, almost no CO_2 ($\psi_{CO_2} < 0.05\%$) and very little CO and HC emissions, which occur at a level of $\psi_{CO,HC} < 15$ ppm, are present. In diesel engines CO_2 can be found in concentrations of $\psi_{CO_2} \geq 8\%$ in the exhaust gas [29]. Diesel engines furthermore produce CO emissions in the raw exhaust from $\psi_{CO} = 150$ ppm to 1400 ppm and HC species can be found up to $\psi_{HC} = 750$ ppm [30]. Second, the water content is on a higher level ranging up to $\psi_{H_2O} = 25\%$ during the cold-started driving cycles which is significantly higher compared to diesel engines ($\psi_{H_2O} \approx 8\%$) [29]. Third, as the engine was converted to hydrogen operation, it is not fully optimized and some unburned hydrogen can be found in the exhaust gases. Last but not least, the level of NO_x raw emissions is on the remarkably low level below 5 ppm at most of the time, however, during rapid load changes, NO_x peaks with magnitudes of up to $\psi_{NO_x} = 3,000$ ppm can occur during a short time.

Subsequent to the cold-start investigations, a variation of the air-fuel equivalence ratio λ followed as presented in Fig. 2. The experiment

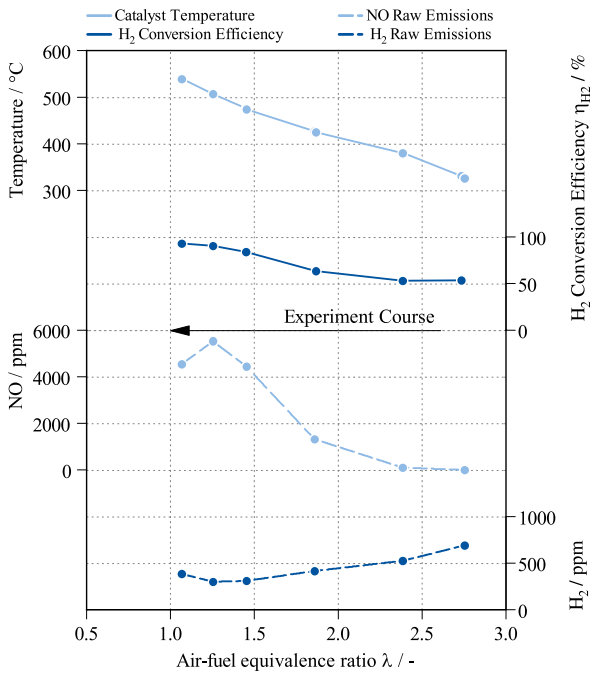

Fig. 2. Catalyst temperature T_{cat}, H_2 conversion efficiency η_{H_2} and NO and H_2 emissions at a variation of the air-fuel equivalence ratio λ from lean towards stoichiometric operation; engine test bench operated at $n_{eng} = 1500\,min^{-1}$ and $BMEP_{eng} = 8\,bar$.

commenced with an air-fuel equivalence ratio $\lambda > 2.5$, which subsequently decreases. To achieve this, the use of the variable turbine geometry (VTG) was lowered in a first step, to diminish the intake air mass while the engine torque and speed was not changed. To achieve a further reduction of the air-fuel equivalence ratio λ in a second step, the engine was throttled by a valve while maintaining engine speed and torque. In all of the load points the MFB_{50} (point of 50% mass fraction burnt) was not changed at all. The air-fuel equivalence ratio reduction resulted in lower O_2 concentrations and an increase in H_2O concentration in the raw exhaust gas. Approaching an air-fuel equivalence ratio of $\lambda = 1$, catalyst temperatures of $T_{Cat} > 500$ °C were recorded. The increase in temperature accelerates the reaction rate of NO_x formation via the Zeldovich mechanism [31], which leads to higher NO_x raw emissions. Overall, the changes in temperature and NO emissions were the most pronounced effects during the variation.

As a result of the lambda variation, the conversion efficiency η_{H_2} of H_2 in the OC rose significantly, namely from an initial value of $\eta_{H_2} = 53.2\%$ to 92.5% at the end of the λ variation experiment. This reactivation implies a reversible nature of the previously observed degradation phenomenon.

However, it is important to recognize that the deactivation of OCs during the operation of H_2-fueled ICEs is a newly identified phenomenon. Addressing this deactivation and finding solutions for reactivation are crucial for lowering H_2 concentrations and ensuring that the OC functions as a safety-critical component in the EAT. These findings may have significant implications for engine operation, as reactivation cycles may need to be integrated to mitigate severe deactivation.

1.3. Approach to explain fast but reversible catalyst deactivation

A review of the literature revealed that a number of mechanisms and species can be involved in the deactivation process of the oxidation catalyst. One mechanism is that hydrogen conversion could lead to exothermic heat release at the active catalytic centers, causing local thermal aging, even at globally low exhaust gas temperatures. However, this would not be reversible [32–34]. A mechanical deposition of CO and HC (coking, fouling) could be reversible, but should be less significant for H_2-ICEs and their low amounts of carbon-based emissions [35].

In case of H_2O, whose concentration is significantly higher in H_2-ICEs compared to diesel engines, some authors attribute a deactivation effect to its presence. In their report, Weiss et al. [36] state that the presence of H_2O can result in the adsorption of nonreactive hydroxyl (OH) on a Pt-loaded catalyst in O_2 atmosphere. This adsorption process results in a loss of activity when H_2O is present, a phenomenon that has also been observed in other oxidation reactions. The effect may be reversible as higher temperatures can lead to the desorption of surface H_2O and the loss of OH groups. Peng and Dawson [37] state that H_2O only adsorbs very weakly on platinum surfaces, but report that this adsorption process is significantly increased in presence of O_2. In order to remove the H_2O from the platinum surface, Unger et al. [38] report that the H_2O desorbs fully above temperatures of $T = 600$ °C.

Olsson and Fridell [39], as well as Hauptmann et al. [40] observed similar degradation on Pt-loaded catalysts and attribute it to the formation of platinum oxides. They investigated Pt-loaded oxidation cataylsts for diesel applications (DOC) during NO oxidation. The chemical-based catalyst deactivation due to formation of platinum oxide is known to be less catalytically acitve than the metallic Pt [39]. Hauff et al. [41] also attribute the deactivation to platinum oxide formation, which should decompose again above $T \geq 350$ °C. Furthermore, the deactivation is assumed to be caused by O_2 and NO_2 in the inlet feed [39]. Hauff et al. [41] found that in the case of O_2 excess, such as in diesel- or H_2-ICE raw exhaust gas, low NO_2 concentrations do not lead to additional deactivation. The authors also observed a reduction of platinum oxide at low temperature by NO. However, they conclude that H_2 is a more effective reducing agent. H_2 reduces Pt oxide (PtO_x) to metallic Pt, while H_2O is produced [42]. Hauptmann et al. [40] suggests a reducing effect on the Pt oxide of a deactivated DOC through hydrocarbons, CO and H_2. Furthermore, the work of Mulla et al. [43] indicates that complete reactivation could be achieved through the exposure of the catalyst to CO or H_2.

Becker et al. [44] identified a poisoning effect of excess O_2 on the methane (CH_4) oxidation on Pt/Al_2O_3 catalysts and emphasized the importance of an optimal surface ratio of Pt and O. Various studies yield similar results [45–47]. The formation of surface oxides is likely to inhibit dissociative adsorption of CH_4, thus reducing the activity for CH_4 oxidation [46]. Various tests in multiple studies indicate, that periodic operation – through switching between lean and rich gas composition – enhances the activity of CH_4 oxidation [44–47]. Futhermore, Carlsson et al. [46] observed that CH_4 oxidation with O_2 excess on Pd/Al_2O_3 is more effective than on Pt/Al_2O_3 catalysts. Fouladvand et al. [48] revealed a significant effect of the support of Pt catalysts on CH_4 oxidation. In two studies, they found that the use of Ce supported Pt catalysts over Pt/Al or Pt/AlCe catalysts yields higher conversion rates, even under lean conditions [47,48].

Based on the facts described above, changes in the platinum oxidation state are the most likely explanations for the observed deactivation phenomenon. We assume that the surface is strongly reduced by H_2, yet a sufficient surface ratio of Pt and O is ensured by the re-oxidizing effect of NO. Therefore, this paper deals with the investigation of the effects of NO concentration (or lack thereof) and of temperature variations on the oxidation catalyst performance.

2. Experimental

2.1. Catalyst specifications and sample preparation

The OC sample used for the investigations is a platinum-based catalyst with a loading of $\rho_{Pt} = 25\ g/ft^3$ on a Al_2O_3 washcoat. The carrier is a state-of-the-art cordierite substrate. The cell density is $\rho_{cat} = 400$ cpsi with a wall thickness of $\delta_{wall} = 4$ mil.

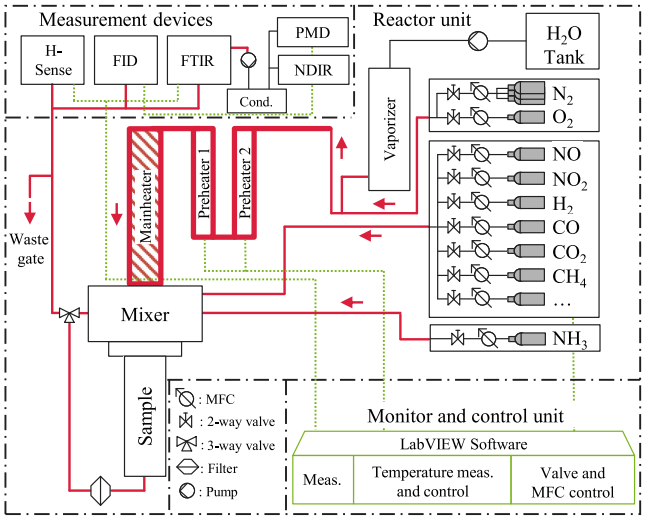

Fig. 3. Experimental setup of the synthetic gas test bench; MFC = Mass flow controller.

For investigations on the SGB (Synthetic gas test bench), a sample is drilled from a fresh monolith. The monolith is part of the same charge of production as the catalyst brick used at the engine test bench. The diameter of the drilled sample measures $d_{sample} = 18.8$ mm with a length of $l_{sample} = 30.2$ mm. Prior to the investigations on the SGB the catalyst was aged for a period of $t_{age} = 10$h at a temperature of $T_{age} = 850$ °C in an $\psi_{H_2O} = 10\%$ content in air atmosphere. The oxygen storage capacity (OSC) of the aged catalyst sample was determined in the range from $OSC_{T=200\ °C} = 0.16$ mmol/l_{cat} to $OSC_{T=400\ °C} = 5.33$ mmol/l_{cat}.

2.2. Laboratory gas test bench setup

The tests to investigate the reversible deactivation of the OC were conducted on the synthetic gas test bench (SGB) of the Chair of Thermodynamics of Mobile Energy Conversion Systems (TME) of RWTH Aachen University under reproducible conditions. The layout of the SGB is shown in Fig. 3. Various gaseous species can be dosed with high precision via the SGB, utilizing different mass flow controllers. Moreover, the evaporation of liquid water in N_2 ensures the water concentration in the synthetic exhaust gas. Further detailed information on the design and equipment of the test bench can be found in the Appendix and previous publications [49,50]. The H_2 concentration was measured using a hydrogen mass spectrometer (HSense). Moreover, additional measurement devices were used to quantify other emissions such as different HC species, NO_x and CO. These include a Fourier-transform infrared spectrometer (FTIR), a flame ionization detector (FID), a paramagnetic detector (PMD), and a non-dispersive infrared sensor (NDIR).

2.3. Light-off test procedure

All light-off investigations included two phases (Fig. 4). The first phase, the conditioning phase, ensured a reproducible, initial state of the catalyst prior to each of the main tests. At the start of the test campaign the conditioning phases were performed at $T_{Cond} = 500$ °C with an upstream concentration of $\psi_{H_2} = 1,000$ ppm in N_2 for a period of $t_{Cond} = 600$ s in order to reduce stored species such as O_2, NO_x and CO. The temperature ramp started at $T_{Start} = 100$ °C with a gradient of $\delta T/\delta t = 10$ K/min. In the later stages of the test campaign, the conditioning phase was conducted at $T_{Cond} = 600$ °C. A gradient of $\delta T/\delta t = 5$ K/min was used to heat the sample from the previous conditioning temperature ($T_{Cond} = 500$ °C) to the target temperature.

Table 2
Gas composition during light-off phase.

Species	Unit	Standard gas matrix	Reduced gas matrix
H_2	ppm	1,000	1,000
NO	ppm	500	–
CO	ppm	25	–
C_3H_8	ppm	10	–
O_2	%	13	13
H_2O	%	15	15

Exhaust gas temperatures of up to $T_{Exhaust} = 600$ °C can be achieved during lean operation of H_2-ICE by adjusting the air-fuel equivalence ratio λ [51]. Moreover, a second dosing phase – the preconditioning – was incorporated in the later stages of the test campaign to the conditioning phase in order to ensure the regeneration of the deactivated OC sample. In the first section of the extended conditioning phase the OC was exposed to NO or CO ($\psi_{NO} = 500$ ppm or $\psi_{CO} = 500$ ppm) in N_2. The first phase of the test ended with the cooling phase in a N_2 atmosphere to the test temperature of $T_{Inlet} = 100$ °C.

In the second phase, referred to as main phase in Fig. 4, the sample was heated up during the light-off to $T_{Inlet} = 500$ °C at a rate of $\delta T/\delta t = 5$ K/min, then the temperature was held for $t = 300$ s. The holding phase was followed by a controlled cooling phase at the same gradient, which is also referred to as the light-out. During the second phase, either the standard or the reduced gas matrix was dosed. For the standard gas matrix, a conservative approach to NO_x and H_2 concentration was used. In addition, a minimal share of CO and C_3H_8 to represent potential oil consumption was calculated based on data from a 2.0 l turbocharged four-cylinder H_2-ICE with direct injection (DI) as presented in [12]. The reduced gas matrix represents a synthetic, NO-free atmosphere. The compositions of both gas matrix variants are presented in Table 2. The gas hourly space velocity was set to $GHSV = 200,000\ h^{-1}$ based on the selection of a small OC for the H_2-ICE, as only minimal amounts of carbon-based emissions need to be oxidized. Moreover, the defined $GHSV$ effectively covers a significant part of the engine's operating range.

3. Results and discussion

3.1. Oxidation catalyst deactivation

In order to identify possible reasons for the deactivation and reactivation of the OC during engine operation, a test series with nine light-off tests was performed on the SGB as shown in Fig. 5, where the H_2 conversion efficiency η_{H_2} is plotted versus the inlet catalyst temperature. The tests were conducted with conditioning applied at $T_{Cond} = 500$ °C and $\psi_{H_2} = 1,000$ ppm. For the main phases of these tests – comprising the light off and light out – the standard and reduced gas compositions described in Table 2 were used. The H_2 conversion efficiency η_{H_2} is calculated according to Eq. (1) (Chapter 1.2).

The intended reproduction of the OC deactivation was achieved during the first test campaign (test series A), as shown by comparing the light-off A1 and A9. A partial higher H_2 conversion efficiency η_{H_2} is achieved up to $T_{Inlet} \approx 210$ °C with the reduced gas matrix. Various studies have addressed the inhibition of different reactions by CO or HC, which is primarily due to adsorption competition on active sites [52,53]. Moreover, Salomons et al. [54] observed an inhibition of H_2 oxidation by CO on a Pt loaded oxidation catalyst. Therefore, the T_{90} light-off temperatures, defined as the temperature at which a H_2 conversion efficiency of $\eta_{H_2} = 90\%$ is achieved, for the tests with the reduced gas matrix are significantly lower than those measured in the tests with the standard gas matrix. The tests performed with the reduced gas matrix led to an accelerated deactivation of the OC in various test campaigns. As the temperature increases up to $T_{Inlet} = 500$ °C, the difference between the conversion efficiencies of the tests

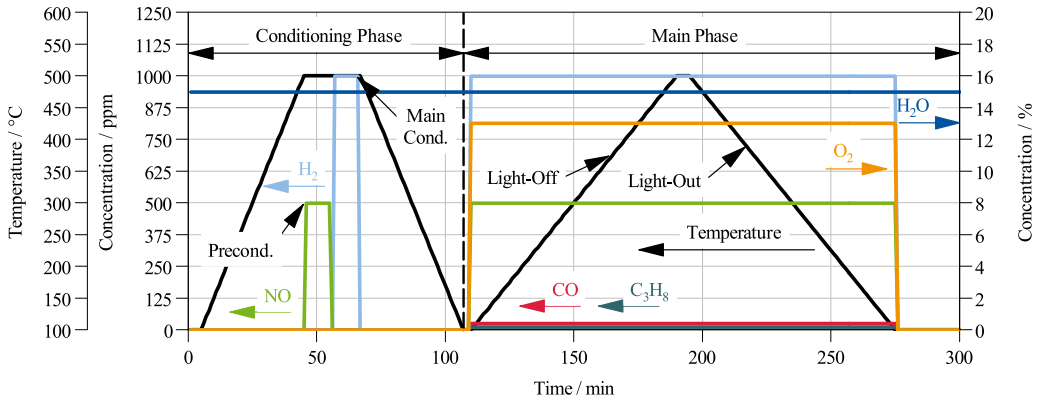

Fig. 4. Test procedure at the synthetic gas test bench with an additional NO conditioning phase at T_{Cond} = 500 °C (heating rate of $\delta T/\delta t$ = 10 K/min up to T_{Cond} = 500 °C) and a standard gas matrix during main phase.

	Conditioning	Light-Off Gas Matrix	T_{50} / °C	T_{90} / °C
A1	H_2 @ 500 °C	Standard	173	230
A2	H_2 @ 500 °C	**Reduced**	-	132
A3	H_2 @ 500 °C	**Reduced**	-	182
A4	H_2 @ 500 °C	Standard	190	286
A5	H_2 @ 500 °C	**Reduced**	-	156
A6	H_2 @ 500 °C	**Reduced**	-	210
A7	H_2 @ 500 °C	Standard	189	307
A8	H_2 @ 500 °C	**Reduced**	-	145
A9	H_2 @ 500 °C	Standard	186	296

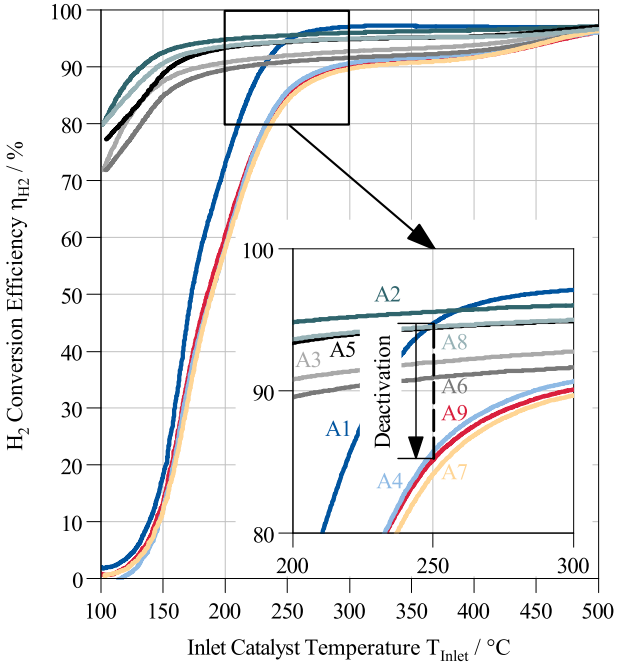

Fig. 5. Temperature-dependent H_2 conversion efficiency η_{H_2} of light-off tests with different gas compositions and conditionings to reproduce oxidation catalyst deactivation (missing T_{50} light-off temperatures due to the start inlet catalyst temperature).

becomes significantly smaller. At this temperature, all conversion rates increase to $\eta_{H_2} \geq 96\%$. However, the H_2 conversion efficiency η_{H_2} from the light-off A1 to A9 is reduced by up to $\Delta\eta_{H_{2,A1\rightarrow A9}} = -10\%$ at a temperature of T_{Inlet} = 250 °C and the T_{90} light-off temperature is increased by $\Delta T_{90,A1\rightarrow A9}$ = 64 °C in a short period of time. The difference in H_2 conversion efficiency $\Delta\eta_{H_2}$ is calculated using Eq. (2).

$$\Delta\eta_{H_{2,x\rightarrow x+i}} = \eta_{H_{2,x+i}} - \eta_{H_{2,x}} \quad (2)$$

Moreover, the change of the T_{90} light-off temperature ΔT_{90} is defined in Eq. (3). The difference of the T_{50} light-off temperature ΔT_{50} is calculated analogously to Eq. (3).

$$\Delta T_{90,x\rightarrow x+i} = T_{90,x+i} - T_{90,x} \quad (3)$$

The test series confirms the significant deactivation observed earlier at the engine test bench (Chapter 1.2).

Further light-off tests were started between light-off A7 and A8. However, these were terminated due to a controller malfunction and are therefore not included in Fig. 5. A comparison of curve A7 and A9 shows no significant influence of tests in between.

3.2. Regeneration of the oxidation catalyst

The results at the engine test bench indicate a reversible nature of the OC deactivation, as a lambda variation leads to increased catalyst efficiency (Chapter 1.2). As the changes in exhaust gas temperature and in the NO concentration were identified as strongest effect of the lambda variation, the following experiments are defined:

1. Dosing of an additional species as a preconditioning
2. Increasing conditioning temperature during the conditioning phase

3.2.1. Dosing of an additional species during the extended conditioning phase

Two different species were applied as a preconditioning species for the OC sample during the extended conditioning phase. The raw exhaust gas of a diesel engine contains a considerable amount of CO, due to the fact that diesel is a carbon containing fuel. In H_2-ICEs, CO forms in much smaller amounts, mainly from engine oil combustion. Thus, the influence of CO on the conditioning and reactivation processes was investigated using the previously deactivated OC. Subsequently, NO was used as a further species in the preconditioning, since the lambda variation is correlated with an increase in NO_x raw emissions in addition to an increase in exhaust gas temperature.

Fig. 6 shows a test series extending the previous deactivation tests. Thus, the light-off tests ***"Additional Investigations"*** can be seen in Fig. 5. The additional light-off tests were **also** performed at a conditioning temperature of T_{Cond} = 500 °C. While the main conditioning stayed the same, the preconditioning of the light-off A10 was conducted with an upstream concentration of ψ_{CO} = 500 ppm and the preconditioning of the test A11 with an upstream concentration of ψ_{NO} = 500 ppm for an additional time of t_{Cond} = 600 s. The concentration of NO is set to ψ_{NO} = 500 ppm, given that the engine is operated at an air-fuel

	Conditioning	Light-Off Gas Matrix	T_{50} / °C	T_{90} / °C
A1	H_2 @ 500 °C	Standard	173	230
	Additional Investigations			
A9	H_2 @ 500 °C	Standard	186	296
A10	CO + H_2 @ 500 °C	Standard	182	260
A11	NO + H_2 @ 500 °C	Standard	181	247

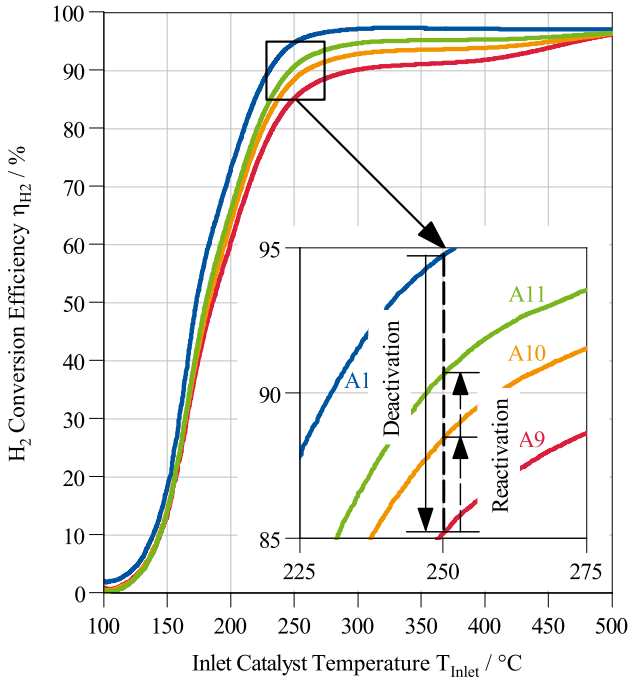

Fig. 6. Temperature-dependent H_2 conversion efficiency η_{H_2} of light-off tests with different preconditionings to reactivate the deactivated oxidation catalyst.

	Conditioning	Light-Off Gas Matrix	T_{50} / °C	T_{90} / °C
A1	H_2 @ 500 °C	Standard	173	230
A9	H_2 @ 500 °C	Standard	186	296
B1	NO + H_2 @ 500 °C	Standard	180	240
B2	H_2 @ 500 °C	**Reduced**	-	142
B3	H_2 @ 500 °C	**Reduced**	-	210
B4	H_2 @ 500 °C	Standard	188	281
B5	NO + H_2 @ 500 °C	Standard	186	256
B6	NO + H_2 @ 500 °C	Standard	184	248
B7	NO + H_2 @ 500 °C	Standard	184	246
B8	NO + H_2 @ 500 °C	Standard	184	247

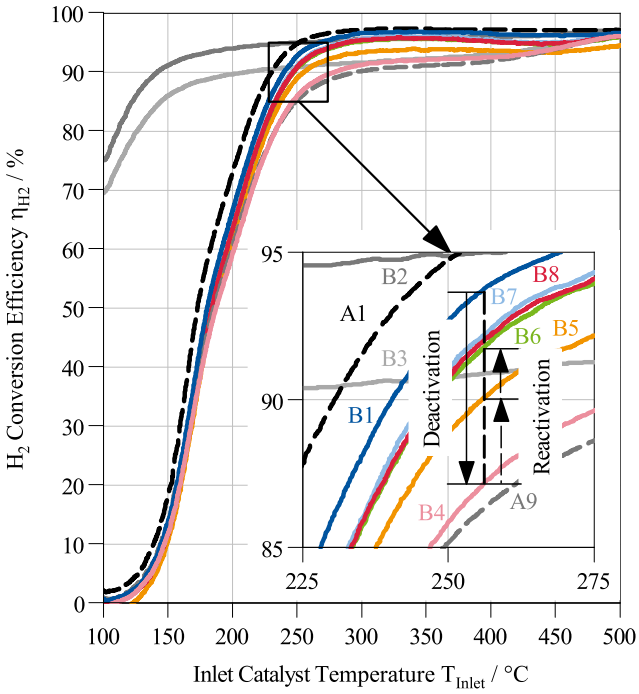

Fig. 7. Temperature-dependent H_2 conversion efficiency η_{H_2} of light-off tests with NO preconditioning to reactivate the deactivated oxidation catalyst (missing T_{50} light-off temperatures due to the start inlet catalyst temperature).

equivalence ratio of $\lambda > 2$ for most load points. Moreover, the CO concentration is selected for a potential comparison to diesel exhaust gas and is not achieved during H_2-ICE operation. During the main phase of both tests the standard gas matrix was used.

The first light-off test with the extended conditioning phase (A10), comprising the preconditioning with CO and the main conditioning with H_2, yields a significant improvement in H_2 conversion efficiency η_{OC} from temperatures of $T_{Inlet} \approx 200$ °C onward through reactivation. Furthermore, the last light-off test A11 of this test series with the NO preconditioning shows further improved H_2 conversion efficiency η_{H_2}. Both reactivation attempts result in a cumulative increase in H_2 conversion efficiency η_{H_2} of up to $\Delta\eta_{H_2,A9\rightarrow A11} = 6\%$ at a temperature of $T_{Inlet} = 250$ °C. The T_{90} light-off temperature drops significantly by $\Delta T_{90,A9\rightarrow A11} = 49$ °C to $T_{90,A11} = 247$ °C. The T_{50} temperature is effected less. The tests indicate that both preconditionings – with CO and NO – result in a reactivation of the OC. However, the reactivation of the OC to a H_2 conversion efficiency η_{H_2} as high as the initial efficiency was not achieved.

A second test series (test series B) was performed to determine the maximum reactivation of the OC. This time, only NO is considered, due to its higher relevance for H_2-ICE applications, as NO_x emissions represent a more significant pollutant in H_2-ICE compared to carbon-based emissions. The test series began with a reference light-off test, with the extended conditioning comprising $\psi_{NO} = 500$ ppm as preconditioning and $\psi_{H_2} = 1,000$ ppm as the main conditioning. In order to deactivate the OC sample, two light-off tests with H_2 conditioning were performed using the reduced gas matrix in the main phase. Four consecutive light-off tests with a preconditioning at $\psi_{NO} = 500$ ppm and $T_{Cond} = 500$ °C were conducted on the previously deactivated OC sample, as shown in Fig. 7.

The intentional deactivation via the light-off tests with reduced gas matrix in the main phase leads to an expected decrease in H_2 conversion efficiency, as indicated by comparing the T_{50} and T_{90} light-off temperatures of the test B1 and B4. An increase of $\Delta T_{50,B1\rightarrow B4} = 8$ °C and $\Delta T_{90,B1\rightarrow B4} = 41$ °C is measured. Moreover, a significant reduction in the H_2 conversion efficiency can already be observed between the two light-off tests performed with the reduced gas matrix. This confirms the results of Fig. 5 and shows that the deactivation with the reduced gas matrix is reproducible.

A further test, this time utilizing preconditioning with NO and main conditioning with H_2, results in an increase in H_2 conversion efficiency, as previously seen in Fig. 6. At $T_{Inlet} = 250$ °C the conversion efficiency improves by up to $\Delta\eta_{H_2,B4\rightarrow B5} = 3\%$. The repetition of this test leads to a further improvement of the H_2 conversion efficiency by $\Delta\eta_{H_2,B5\rightarrow B6} = 2\%$. However, light-off B7 and B8, which have also been pre-conditioned with NO, are almost in line with test B6. These results show, that one repetition of the light-off test with the NO preconditioning leads to a reactivation of the OC sample to a certain extent. However, further repetition does not lead to a significant additional improvement. The initial H_2 conversion efficiency was not restored through a combination

of an upstream concentration of ψ_{NO} = 500 ppm and ψ_{H_2} = 1,000 ppm at T_{Cond} = 500 °C in an extended conditioning phase.

3.2.2. Increase of the conditioning phase temperature

During lambda variations, the exhaust gas temperature rises due to the enrichment of the charge and the accompanying increase in temperature within the combustion chamber. Thus, as an alternative to dosing an additional species, the temperature of the conditioning of the OC sample was increased by ΔT_{Cond} = 100 °C to T_{Cond} = 600 °C. Fig. 8 displays the H_2 conversion efficiency of the OC over the inlet catalyst temperature during light-off tests (test series C) performed with a main conditioning at a temperature of T_{Cond} = 600 °C and an upstream H_2 concentration of ψ_{H_2} = 1,000 ppm. The first light-off (C1) of the test series C is presented solely as a reference for the test series shown and is not subjected to further analysis. Furthermore, ***"Additional Investigations"*** refers to three additional tests that were conducted prior to this test series, which are also not the focus of this test campaign. The first of these three tests involved a shortened preconditioning phase with H_2 lasting t = 150 s, followed by a light-off using the reduced gas matrix. The second test consists of a light-off with the standard gas matrix after a H_2-only preconditioning. In the third test, the preconditioning is modified to start with H_2, followed by a preconditioning with O_2 with an upstream concentration of ψ_{O_2} = 13% for a period of t = 2,400 s, and concluding with a light-off using the standard gas matrix.

An additional preconditioning with CO or NO as implemented in both test series in Section 3.2.1 was not conducted in this test series. With the exception of the test C6, the standard gas matrix was dosed in each of the main phases. To assess the effect of the absence of NO, CO and C_3H_8 following the high-temperature conditioning, as well as to serve as a comparison to the tests conducted with conditioning at a temperature of T_{Cond} = 600 °C, the light-off test C6 was performed utilizing the reduced gas matrix in the inlet feed.

The H_2 conversion efficiency of the six light-off tests, except for the second light-off (C6), are nearly identical. As illustrated in the zoomed-in section in Fig. 8, the temperature range from T_{Inlet} = 237.5 °C–250 °C indicates a maximum deviation in H_2 conversion efficiency of $\Delta\eta_{H_{2,C5\rightarrow C10}} < 2.5\%$. Furthermore, the light-off tests conducted subsequent to the test with the reduced gas matrix reveal a minor increase in T_{90} light-off temperature of $\Delta T_{90,C5\rightarrow C10} \leq 10$ °C in comparison to the first light-off of the test series, whereas the deviation of the T_{50} light-off temperature is even smaller. The second light-off test, performed with the reduced gas matrix in the inlet feed, yielded high H_2 conversion efficiency at an earlier stage, as anticipated due to the absence of NO, CO and C_3H_8. From the catalyst inlet temperature of $T_{Inlet} \geq 266$ °C, all H_2 conversion efficiencies exceed $\eta_{H_2} > 97.9\%$.

A detailed comparison between the test campaign in Section 3.2.1 and the test series of Fig. 8 reveals that both the T_{50} and T_{90} light-off temperatures are significantly lower for all light-off tests when conditioning at T_{Cond} = 600 °C with an upstream H_2 concentration of ψ_{H_2} = 1,000 ppm. This high-temperature conditioning consistently results in substantially improved H_2 conversion efficiency across multiple tests, with only minor indications of deactivation. At this point, it has to be mentioned that all results presented in this paper are part of a larger test campaign. The experiments were conducted in chronological order, as follows: The campaign started with Fig. 8, followed by 5 and 6, and subsequently, Fig. 7, all test campaigns with other measurements in between. A comparison of the reference curves (A1) in all graphs suggests a small irreversible deactivation over the course of the overall test campaign. Looking at the rather high exhaust temperatures compared to standard diesel applications, a thermal nature of the degradation seems plausible.

	Conditioning	Light-Off Gas Matrix	T_{50} / °C	T_{90} / °C
A1	H_2 @ 500 °C	Standard	173	230
A9	H_2 @ 500 °C	Standard	186	296
C1	NO + H_2 @ 600 °C	Standard	180	221
.....	***Additional Investigations***			
C5	H_2 @ 600 °C	Standard	170	211
C6	H_2 @ 600 °C	**Reduced**	-	122
C7	H_2 @ 600 °C	Standard	172	219
C8	H_2 @ 600 °C	Standard	171	218
C9	H_2 @ 600 °C	Standard	172	221
C10	H_2 @ 600 °C	Standard	172	221

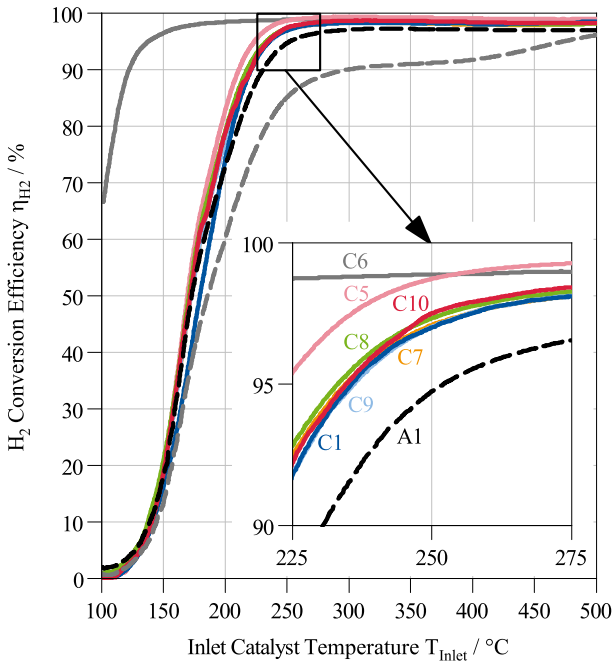

Fig. 8. Temperature-dependent H_2 conversion efficiency η_{H_2} of light-off tests with a conditioning temperature of T_{Cond} = 600 °C (missing T_{50} light-off temperature due to the start inlet catalyst temperature).

4. Conclusions

Longer cold start and low load operation at the engine test bench caused a deactivation of the oxidation catalyst. With hydrogen as a fuel, the aging was comparably high to diesel experience. However, a reduction of the relative air-fuel equivalence ratio at constant load, resulting in increased exhaust gas temperature and nitrogen oxide emissions, led to a reactivation of the catalyst. The results indicate a new, partly reversible aging phenomenon specific to hydrogen engines, not observed in diesel applications. Key differences from diesel exhaust include higher water content, some raw hydrogen emissions, minimal carbon dioxide, and very low levels of carbon monoxide, hydrocarbons, particulate matter, and nitrogen oxides.

A similar deactivation of an oxidation catalyst from the same production batch could be proven at the synthetic gas test bench (SGB), when applying a reduced gas matrix. Here, only hydrogen, oxygen, water and nitrogen, but no pollutant emissions were present. A conditioning of t_{Cond} = 600 s phase at T_{Cond} = 500 °C under hydrogen-containing atmosphere was supposed to provide similar catalyst characteristics upfront each light-off test. Besides hydrogen, the conditioning atmosphere contained water, but no oxygen. Since hydrogen is a highly reactive reducing agent, one would expect it to reduce the catalyst surface. Still the deactivation was observed.

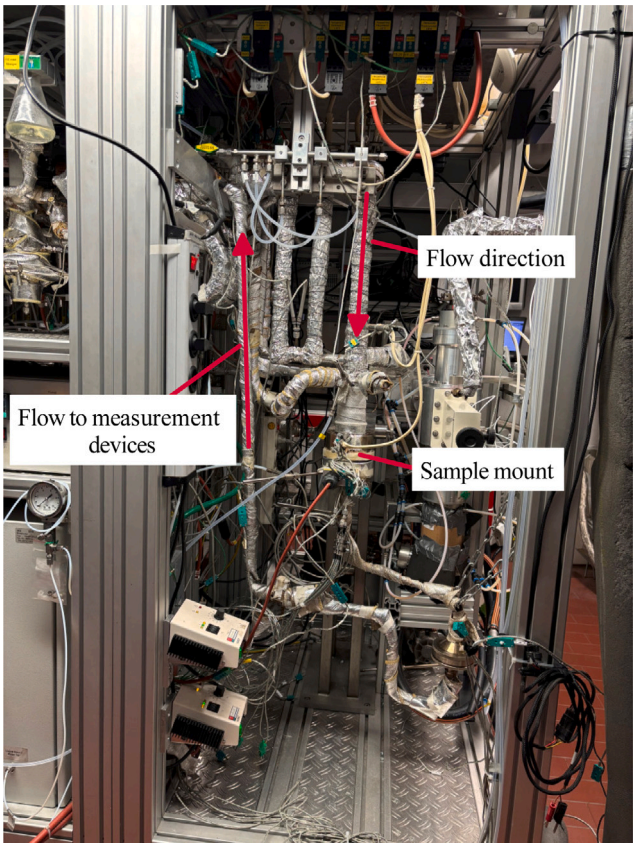

Fig. 9. Setup of the synthetic gas test bench used.

Adding nitrogen oxide to the conditioning phase enables a reactivation of the catalyst activity. Thus, nitrogen oxide initiates some changes in the catalyst condition that were not present with hydrogen. A similar reactivation effect was observed for carbon monoxide, which usually is present in significantly higher concentration in diesel ICE exhaust compared to hydrogen engines. As an alternative to NO or CO in the conditioning, an increased temperature of $T_{\mathrm{Cond}} = 600$ °C during the (hydrogen-only) conditioning was also able to reactivate the catalyst or to potentially prevent the catalyst from deactivation.

The investigations on the engine test bench and the synthetic gas test bench led to the following basic findings and conclusions:

- A reversible catalyst deactivation phenomenon of a state-of-the-art oxidation catalyst, originally designed for diesel applications, is reproducible in hydrogen combustion engines at the synthetic gas test bench.
- Nitrogen oxide positively influences hydrogen oxidation activity. However, with a conditioning temperature of $T_{\mathrm{Cond}} = 500$ °C, the reactivation stagnates towards a conversion level below the initial curve.
- The conditioning at $T_{\mathrm{Cond}} = 600$ °C significantly prevents deactivation. With reduced light-off temperatures, the deactivation is more powerful than with the $T_{\mathrm{Cond}} = 500$ °C variant, independently of the presence of NO emissions.
- The water concentration was on a constant level of $\psi_{\mathrm{H_2O}} = 15\%$ representing hydrogen ICE exhaust gas conditions during all conditioning and light-off experiments. Future work will investigate the impact of varying water concentrations on catalyst deactivation.

The following conclusions for the application of oxidation catalysts in the exhaust aftertreatment system of hydrogen combustion engines can be derived from the findings of this study:

- If engines are operated ultra-lean, there are only minimal amounts of NO_x present in the raw exhaust gas, which can result in the deactivation of the oxidation catalyst over time.
- Based on the findings presented in this study, we recommend an exhaust gas temperature of $T > 500$ °C and a NO concentration of at least $\psi_{\mathrm{NO}} = 500$ ppm to induce regeneration effects. Achieving temperatures of up to $T = 600$ °C may be limited by practical factors. To achieve this threshold, either high loads are suitable or, based on our findings, temporarily reducing the relative air-fuel equivalence ratio to $\lambda < 1.5$.

In summary, state-of-the-art OCs as known from diesel engines are applicable for the use in H_2-ICEs, if the catalyst deactivation observed with the tested type of OC is taken into account through suitable engine operating modes. As neither the engine nor the catalyst were optimized for hydrogen applications, further improvement is expected, e.g. resulting in lower hydrogen raw emissions or higher aging resistance.

CRediT authorship contribution statement

Alexander Lampkowski: Investigation, Writing – original draft, Conceptualization. **Stefan Sterlepper:** Conceptualization, Writing – review & editing. **Maike Schäfer:** Investigation. **Sebastian Roiser:** Investigation, Writing – original draft, Conceptualization. **Christian Tomanik:** Writing – review & editing. **Helmut Eichlseder:** Writing – review & editing, Supervision. **Stefan Pischinger:** Writing – review & editing, Supervision.

Funding

This research project 1449 “Near-zero emission concept for high-efficiency hydrogen engine with direct injection” was funded by FVV e.V..

Declaration of competing interest

The authors declare that they have no known competing financial interests or personal relationships that could have appeared to influence the work reported in this paper.

Acknowledgments

The authors would particularly like to thank all members of the FVV working group 1449 for their helpful feedback, ideas and discussions, as well as Claus Wundling and David Lejsek (both Robert Bosch GmbH) for their chairmanship. Special thanks are also expressed to Umicore AG & Co. KG for providing the catalyst components required for the investigations.

Appendix

This section provides a detailed overview of the synthetic gas test bench setup. The sample is installed in the test bench using a canning system, as illustrated in Fig. 9. Gases are supplied from gas cylinders through a pressure regulator set to $p = 5$ bar. To achieve the desired concentrations upstream of the catalyst sample, closed-loop controlled mass flow controllers (MFCs) with varying volume flows from Brooks Instrument LLC are employed. In order to prevent unintended gas dosing into the test bench, additional solenoid valves made by Christian Bürkert GmbH & Co. KG are installed after each MFC. The required water concentration is achieved by evaporating liquid water, with precise dosing managed by a Cetoni Nemesys S syringe pump. Upstream of the catalyst sample, the gas is heated to the required temperature using heaters. For emission analysis, hydrogen mass spectrometer (HSense) from V&F Analyse- und Messtechnik GmbH is used for H_2

concentration measurements and Fourier-transform infrared spectrometer (FTIR) measurements are performed using an MKS MultiGas 2030 from MKS Instruments, Inc. Standard measuring devices such as PMD and NDIR provided by FEV Europe GmbH, which includes a Thermo-FID from SK-Elektronik GmbH. To prevent condensation of gases, the pipes leading to the measurement devices are heated. Gas dosages and concentrations are verified before and after each experiment using a bypass measurement that circumvents the catalyst sample.

References

[1] Verhelst Sebastian, Wallner Thomas. Hydrogen-fueled internal combustion engines. Prog Energy Combust Sci 2009;35(6):490–527. http://dx.doi.org/10.1016/j.pecs.2009.08.001.

[2] Verhelst S. Recent progress in the use of hydrogen as a fuel for internal combustion engines. Int J Hydrog Energy 2014;39(2):1071–85. http://dx.doi.org/10.1016/j.ijhydene.2013.10.102.

[3] Onorati A, Payri R, Vaglieco BM, Agarwal AK, Bae C, Bruneaux G, et al. The role of hydrogen for future internal combustion engines. Int J Engine Res 2022;23(4):529–40. http://dx.doi.org/10.1177/14680874221081947.

[4] Verhelst Sebastian, Turner James WG. Hydrogen-fueled spark ignition engines. In: Hydrogen for future thermal engines. Springer International Publishing; 2023, p. 329–51.

[5] Chen Yajuan, Lou Diming, Zhang Yunhua, Fang Liang, Yang Dongxia, Ren Dezhi, et al. An investigation on the H2o, unburned H2 and NO emission characteristics from a direct injection hydrogen engine. Int J Hydrog Energy 2024;81:1181–91. http://dx.doi.org/10.1016/j.ijhydene.2024.07.368.

[6] Luo Qing-he, Hu Ji-Bin, Sun Bai-gang, Liu Fu-shui, Wang Xi, Li Chao, et al. Experimental investigation of combustion characteristics and nox emission of a turbocharged hydrogen internal combustion engine. Int J Hydrog Energy 2019;44(11):5573–84. http://dx.doi.org/10.1016/j.ijhydene.2018.08.184.

[7] Srisailam Shravan Kumar, Patchett Joe, Wu Ralph, Wang Lu, Shah Sandip, Tang Weiyong. Exhaust after treatment solution for H2-ICE for selective NOx removal in the presence of high amount of water content. SAE Int J Adv Curr Pr Mobil 2024. http://dx.doi.org/10.4271/2024-26-0146.

[8] Rezaei Reza, Kovacs David, Hayduk Christopher, Mennig Marian, Delebinski Thaddaeus. Euro VII and beyond with hydrogen combustion for commercial vehicle applications: From concept to series development. SAE Int J Adv Curr Pr Mobil 2021;4(2):559–69. http://dx.doi.org/10.4271/2021-01-1196.

[9] Borchers Michael, Lott Patrick, Deutschmann Olaf. Selective catalytic reduction with hydrogen for exhaust gas after-treatment of hydrogen combustion engines. Top Catal 2023;66:973–84. http://dx.doi.org/10.1007/s11244-022-01723-1.

[10] Eßer Enno, Müller Kim, Kureti Sven. Low-temperature H2-denox in diesel exhaust. Top Catal 2023;66(13–14):1020–30. http://dx.doi.org/10.1007/s11244-022-01719-x.

[11] Guan Yu, Liu Yinhe, Lv Qiang, Wang Bo, Che Defu. Review on the selective catalytic reduction of NOx with H2 by using novel catalysts. J Environ Chem Eng 2021;9(6):106770. http://dx.doi.org/10.1016/j.jece.2021.106770.

[12] Özyalcin Can, Sterlepper Stefan, Roiser Sebastian, Eichlseder Helmut, Pischinger Stefan. Exhaust gas aftertreatment to minimize NOX emissions from hydrogen-fueled internal combustion engines. Appl Energy 2024;353:122045. http://dx.doi.org/10.1016/j.apenergy.2023.122045.

[13] Berg Victor, Koopmans Lucien, Sjöblom Jonas, Dahlander Petter. Characterization of gaseous and particle emissions of a direct injection hydrogen engine at various operating conditions. SAE Int J Adv Curr Pr Mobil 2023;6(3):1746–57. http://dx.doi.org/10.4271/2023-32-0042.

[14] Forzatti Pio, Lietti Luca, Nova Isabella, Tronconi Enrico. Diesel NOx aftertreatment catalytic technologies: Analogies in LNT and SCR catalytic chemistry. Catal Today 2010;151(3–4):202–11. http://dx.doi.org/10.1016/j.cattod.2010.02.025.

[15] Koebel M, Madia G, Elsner M. Selective catalytic reduction of NO and NO2 at low temperatures. Catal Today 2002;73(3):239–47. http://dx.doi.org/10.1016/S0920-5861(02)00006-8, Environmental Catalysis.

[16] Nova Isabella, Tronconi Enrico. Urea-SCR technology for denox after treatment of diesel exhausts. New York, NY: Springer New York; 2014, http://dx.doi.org/10.1007/978-1-4899-8071-7.

[17] Koebel M, Elsener M, Kleemann M. Urea-SCR: a promising technique to reduce NOx emissions from automotive diesel engines. Catal Today 2000;59(3):335–45. http://dx.doi.org/10.1016/S0920-5861(00)00299-6.

[18] Pochet Maxime, Jeanmart Hervé, Contino Francesco. Uncertainty quantification from raw measurements to post-processed data: A general methodology and its application to a homogeneous-charge compression–ignition engine. Int J Engine Res 2020;21(9):1709–37. http://dx.doi.org/10.1177/1468087419892697.

[19] Peters Nathan, Bunce Michael. Lambda determination challenges for ultra-lean hydrogen-fueled engines and the impact on engine calibration. SAE Int J Adv Curr Pr Mobil 2023. http://dx.doi.org/10.4271/2023-01-0286.

[20] Roiser Sebastian, Beringer Stefan, Schutting Eberhard, Eichlseder Helmut, Rabe Tobias, Krinn Ilona, et al. Driving hydrogen engines towards a zero-impact emission level. In: Heintzel Alexander, editor. Internationaler motorenkongress 2023. Wiesbaden: Springer Fachmedien Wiesbaden; 2024, p. 17–37.

[21] Bartholomew Calvin H. Mechanisms of catalyst deactivation. Appl Catal A: Gen 2001;212(1):17–60. http://dx.doi.org/10.1016/S0926-860X(00)00843-7, Catalyst Deactivation.

[22] Forzatti Pio, Lietti Luca. Catalyst deactivation. Catal Today 1999;52(2):165–81. http://dx.doi.org/10.1016/S0920-5861(99)00074-7.

[23] Crabtree Robert H. Deactivation in homogeneous transition metal catalysis: Causes, avoidance, and cure. Chem Rev 2015;115(1):127–50. http://dx.doi.org/10.1021/cr5004375, PMID: 25493420.

[24] Deutschmann Olaf, Knözinger Helmut, Kochloefl Karl, Turek Thomas. Heterogeneous catalysis and solid catalysts. In: Ullmann's encyclopedia of industrial chemistry. John Wiley & Sons, Ltd; 2009.

[25] Argyle Morris D, Bartholomew Calvin H. Heterogeneous catalyst deactivation and regeneration: A review. Catalysts 2015;5(1):145–269. http://dx.doi.org/10.3390/catal5010145.

[26] Trimm DL. Introduction to catalyst deactivation. In: Figueiredo José Luís, editor. Progress in catalyst deactivation. Dordrecht: Springer Netherlands; 1982, p. 3–22.

[27] Trimm DL. Deactivation and regeneration. In: Handbook of heterogeneous catalysis. John Wiley & Sons, Ltd; 1997, p. 1263–82. http://dx.doi.org/10.1002/9783527619474.ch7.

[28] Roiser Sebastian, Christoforetti Paul, Schutting Eberhard, Eichlseder Helmut. Emission behaviour and aftertreatment of stationary and transient operated hydrogen engines. Int J Engine Res 2024;25(2):334–46. http://dx.doi.org/10.1177/14680874231172316.

[29] Merker Günter P, Teichmann Rüdiger. Grundlagen verbrennungsmotoren. Wiesbaden: Springer Fachmedien Wiesbaden; 2019, http://dx.doi.org/10.1007/978-3-658-23557-4.

[30] Pischinger Rudolf, Klell Manfred, Sams Theodor. Thermodynamik der verbrennungskraftmaschine. Vienna: Springer Vienna; 2010, http://dx.doi.org/10.1007/978-3-211-99277-7.

[31] Heywood John B. Internal combustion engine fundamentals. Mcgraw-hill; 1988.

[32] Wiebenga Michelle H, Kim Chang Hwan, Schmieg Steve J, Oh Se H, Brown David B, Kim Do Heui, et al. Deactivation mechanisms of Pt/Pd-based diesel oxidation catalysts. Catal Today 2012;184(1):197–204. http://dx.doi.org/10.1016/j.cattod.2011.11.014, Catalytic Control of Lean-Burn Engine Exhaust Emissions.

[33] Andersson Jonas, Antonsson Matilda, Eurenius Lisa, Olsson Eva, Skoglundh Magnus. Deactivation of diesel oxidation catalysts: Vehicle- and synthetic aging correlations. Appl Catal B: Environ 2007;72(1):71–81. http://dx.doi.org/10.1016/j.apcatb.2006.10.011.

[34] Auvray Xavier, Pingel Torben, Olsson Eva, Olsson Louise. The effect gas composition during thermal aging on the dispersion and NO oxidation activity over Pt/Al2o3 catalysts. Appl Catal B: Environ 2013;129:517–27. http://dx.doi.org/10.1016/j.apcatb.2012.10.002.

[35] Lott Patrick, Wagner Uwe, Koch Thomas, Deutschmann Olaf. Der Wasserstoffmotor – Chancen und Herausforderungen auf dem Weg zu einer dekarbonisierten Mobilität. Chem Ing Tech 2022;94(3):217–29. http://dx.doi.org/10.1002/cite.202100155.

[36] Weiss Brian M, Iglesia Enrique. Mechanism and site requirements for NO oxidation on Pd catalysts. J Catalysis 2010;272(1):74–81. http://dx.doi.org/10.1016/j.jcat.2010.03.010.

[37] Dawson PT, Peng YK. The adsorption, desorption, and exchange reactions of oxygen, hydrogen, and water on platinum surfaces. Surf Sci 1980;92(1):1–13. http://dx.doi.org/10.1016/0039-6028(80)90238-1.

[38] Ungerer Marietjie J, Santos-Carballal David, Cadi-Essadek Abdelaziz, van Sittert Cornelia GCE, de Leeuw Nora H. Interaction of H2O with the platinum pt (001), (011), and (111) surfaces: A density functional theory study with long-range dispersion corrections. J Phys Chem C, Nanomater Interfaces 2019;123(45):27465–76. http://dx.doi.org/10.1021/acs.jpcc.9b06136.

[39] Olsson Louise, Fridell Erik. The influence of pt oxide formation and pt dispersion on the reactions NO2<->no+1/2 O2 over Pt/Al2o3 and Pt/Bao/Al2o3. J Catalysis 2002;210(2):340–53. http://dx.doi.org/10.1006/jcat.2002.3698.

[40] Hauptmann W, Votsmeier M, Gieshoff J, Drochner A, Vogel H. Inverse hysteresis during the NO oxidation on pt under lean conditions. Appl Catal B: Environ 2009;93(1):22–9. http://dx.doi.org/10.1016/j.apcatb.2009.09.008.

[41] Hauff K, Tuttlies U, Eigenberger G, Nieken U. Platinum oxide formation and reduction during NO oxidation on a diesel oxidation catalyst – experimental results. Appl Catal B: Environ 2012;123–124:107–16. http://dx.doi.org/10.1016/j.apcatb.2012.04.008.

[42] Kikkawa Soichi, Teramura Kentaro, Asakura Hiroyuki, Hosokawa Saburo, Tanaka Tsunehiro. In situ time-resolved XAS study on metal-support-interaction-induced morphology change of PtO2 nanoparticles supported on γ-Al2o3 under H2 reduction. Catal Today 2023;410. http://dx.doi.org/10.1016/j.cattod.2022.02.012.

[43] Mulla SS, Chen N, Cumaranatunge L, Blau GE, Zemlyanov DY, Delgass WN, et al. Reaction of NO and O2 to NO2 on pt: Kinetics and catalyst deactivation. J Catalysis 2006;241(2):389–99. http://dx.doi.org/10.1016/j.jcat.2006.05.016.

[44] Becker Elin, Carlsson Per-Anders, Grönbeck Henrik, Skoglundh Magnus. Methane oxidation over alumina supported platinum investigated by time-resolved in situ XANES spectroscopy. J Catalysis 2007;252(1):11–7. http://dx.doi.org/10.1016/j.jcat.2007.09.004.

[45] Becker Elin, Carlsson Per-Anders, Kylhammar Lisa, Newton Mark A, Skoglundh Magnus. In situ spectroscopic investigation of low-temperature oxidation of methane over alumina-supported platinum during periodic operation. J Phys Chem C 2011;115(4):944–51. http://dx.doi.org/10.1021/jp103609n.

[46] Carlsson Per-Anders, Fridell Erik, Skoglundh Magnus. Methane oxidation over Pt/Al2o3 and Pd/Al2o3 catalysts under transient conditions. Catal Lett 2007;115(1–2):1–7. http://dx.doi.org/10.1007/s10562-007-9057-1.

[47] Fouladvand Sheedeh, Skoglundh Magnus, Carlsson Per-Anders. Unsteady-state operation of supported platinum catalysts for high conversion of methane. Chem Eng J 2016;292:321–5. http://dx.doi.org/10.1016/j.cej.2016.02.033.

[48] Fouladvand Sheedeh, Skoglundh Magnus, Carlsson Per-Anders. A transient in situ infrared spectroscopy study on methane oxidation over supported pt catalysts. Catal Sci Technol 2014;4(10):3463–73. http://dx.doi.org/10.1039/C4CY00486H.

[49] Özyalcin Can, Mauermann Peter, Dirkes Steffen, Thiele Paul, Sterlepper Stefan, Pischinger Stefan. Investigation of filtration phenomena of air pollutants on cathode air filters for PEM fuel cells. Catalysts 2021;11(11).

[50] Özyalcin Can, Mauermann Peter, Dornseiffer Jürgen, Sterlepper Stefan, Günther Marco, Pischinger Stefan. Contributions of washcoat components in different configurations to the NOX and oxygen storage performance of LNT catalysts. Catalysts 2022;12(9). http://dx.doi.org/10.3390/catal12090953.

[51] Sterlepper Stefan, Fischer Marcus, Claßen Johannes, Huth Verena, Pischinger Stefan. Concepts for hydrogen internal combustion engines and their implications on the exhaust gas aftertreatment system. Energies 2021;14(23). http://dx.doi.org/10.3390/en14238166.

[52] AL-Harbi Meshari, Hayes Robert, Votsmeier Martin, Epling William S. Competitive no, co and hydrocarbon oxidation reactions over a diesel oxidation catalyst. Can J Chem Eng 2012;90(6):1527–38. http://dx.doi.org/10.1002/cjce.20659.

[53] Mazzarino I, Barresi AA. Catalytic combustion of voc mixtures in a monolithic reactor. Catal Today 1993;17(1–2):335–47. http://dx.doi.org/10.1016/0920-5861(93)80037-2.

[54] Salomons S, Votsmeier M, Hayes RE, Drochner A, Vogel H, Gieshof J. CO and H2 oxidation on a platinum monolith diesel oxidation catalyst. Catal Today 2006;117(4):491–7. http://dx.doi.org/10.1016/j.cattod.2006.06.001.